

Topological order parameters of the spin- $\frac{1}{2}$ dimerized Heisenberg ladder in magnetic field

Toshikaze Kariyado* and Yasuhiro Hatsugai†

Division of Physics, Faculty of Pure and Applied Sciences, University of Tsukuba, Tsukuba, Ibaraki 305-8571, Japan

(Received 26 December 2014; revised manuscript received 20 March 2015; published 8 June 2015)

Topological properties of the spin-1/2 dimerized Heisenberg ladder are investigated, focusing on the plateau phase in the magnetic field whose magnetization is half of the saturation value. Although the applied magnetic field removes most of the symmetries of the system, there is a symmetry-protected topological phase supported by the spatial inversion symmetry. The Z_2 Berry phase associated with a symmetry-respecting boundary and quantized into 0 and π is used as a symmetry-protected topological order parameter. Edge states are also analyzed to confirm the bulk-edge correspondence. In addition, a symmetry-breaking boundary is considered. Then, we observe a different type of quantization of the Berry phase, i.e., a quantization into $\pm\pi/2$ of the Berry phase. In this case, the bulk-edge correspondence is also different, namely, there emerge “polarized” edge states for the case with $\pm\pi/2$ quantization. We also evaluate the entanglement entropy by the infinite time-evolving block decimation (iTEBD) to complement the Berry-phase-based arguments. Further, a different type of the topological order parameter is extracted from the matrix product state representation of the ground state given by the iTEBD.

DOI: [10.1103/PhysRevB.91.214410](https://doi.org/10.1103/PhysRevB.91.214410)

PACS number(s): 03.65.Vf, 03.65.Ud

I. INTRODUCTION

The recent use of topology in condensed matter substantially revised our view on the characterization of materials especially for the gapped phases [1–3]. One of the advantages of a topological view is robustness against continuous deformation. One can use a topological quantity to distinguish topological phases since the quantized nature of it guarantees its invariance against continuous deformation [3–5]. Due to the theorem by von Neumann–Wigner, however, a truly generic phase can be a single class since any generic states can be adiabatically connected. Then, the symmetry restriction is essential. The symmetry can be gauge, time reversal, particle hole, reflection, etc. [3,5–7]. When these restrictions give rise to a new nontrivial phase, it is a symmetry-protected topological (SPT) phase. A typical SPT order parameter is the Berry phase, which takes any value without symmetry but can be quantized with the appropriate symmetry.

The continuous deformation, or adiabatic continuation, is also essential for establishing the bulk-edge correspondence [8–11], which is one of the fundamental concepts for characterizing topological phases. Physics at the bulk and the edges are not independent and are related each other, especially for the gapped case. Introduction of a boundary sometimes breaks symmetries of the bulk system, but sometimes does not. From the viewpoint of the symmetry protection, whether or not the edge respects a bulk symmetry has a special importance.

In this paper, the topological properties of a dimerized spin-1/2 Heisenberg ladder with antiferromagnetic coupling are investigated, focusing on the plateau phase at half of the saturation, which we call a 1/2-plateau phase. The 1/2-plateau phase appears in the applied magnetic field, which breaks most of the symmetry of the system. The ladder model itself has been studied extensively [12–18] and some of the studies shed light on the topological aspects of the ladder model [19–21], but the focus has mainly been on the case without magnetic

field. (Very recently, plateau phases at finite magnetization in spin chains have been studied using a SPT viewpoint in Ref. [22].) A main purpose of this paper is to show that the 1/2-plateau phase here is a SPT phase protected by the spatial inversion symmetry that survives even with the finite external magnetic field. The Berry phase and the entanglement entropy are employed to characterize a SPT phase. As we will explain later, boundary shapes are essential for both the Berry phase and the entanglement entropy, and the boundary that keeps the inversion symmetry is mainly used not to destroy the symmetry effects. The importance of the symmetry is also demonstrated by introducing artificial symmetry breaking and by a spontaneous symmetry breaking caused by a ring exchange. We further study edge states to establish the bulk-edge correspondence. In order to complement the above arguments, a boundary that breaks inversion symmetry is also treated. Naively, one may think that such a symmetry-breaking boundary is not useful for characterizing symmetry-protected topological phases. However, for a specific type of symmetry-breaking boundary, we found a different quantization of the Berry phase, i.e., a fractional quantization of the Berry phase into $\pm\pi/2$, instead of the widely observed $0/\pi$ quantization. Further, it is shown that edge states are also unique for the $\pm\pi/2$ -quantization case: there appear “polarized” edge states such that up and down spins are localized at the opposite ends of the finite system. The applied magnetic field is essential for achieving the fractional quantization.

This paper is organized as follows. In Sec. II, a model Hamiltonian and physical quantities used in our topological characterization are introduced. Then, the numerical methods to obtain those physical quantities, i.e., the exact diagonalization and the infinite time-evolving block decimation [23] (iTEBD), are explained. There, we also explain how the topological character of the system is encoded in the matrix product state, in terms of the transformation law against the symmetry operation. Section III contains the main results of this paper. First, the magnetization curve is shown to take a glance at the plateau phase on which we focus in this paper. After that, the topological properties of the 1/2-plateau phase, such as the quantized Berry phase and the bulk-edge

*kariyado@rhodia.ph.tsukuba.ac.jp

†hatsugai@rhodia.ph.tsukuba.ac.jp

correspondence, are discussed in detail. The effects of ring exchange are also considered. Finally, we make a comparison between the 0-plateau phase and the 1/2-plateau phase. The paper is summarized in Sec. IV.

II. MODEL AND METHODS

The model treated in this paper is a dimerized spin-1/2 Heisenberg ladder [15] with the Zeeman field, whose Hamiltonian is written as

$$\hat{H} = \sum_{i=1}^L \sum_{j=1,2} [J_1 \mathbf{S}_{2i,j} \cdot \mathbf{S}_{2i+1,j} + J_2 \mathbf{S}_{2i+1,j} \cdot \mathbf{S}_{2i+2,j}] + J_0 \sum_{i=1}^{2L} \mathbf{S}_{i,1} \cdot \mathbf{S}_{i,2} - B_z \sum_{i=1}^{2L} \sum_{j=1,2} S_{i,j}^z \quad (1)$$

(see Fig. 1). Here, we concentrate on the antiferromagnetic coupling, namely, all of the J s in Eq. (1) are assumed to be positive. For convenience, a parameter Δ is introduced as $\Delta = (J_2 - J_1)/2$. If $\Delta \neq 0$, the minimum unit cell is composed of four spins, while if $\Delta = 0$, it is composed of two. This unit cell structure is essential to obtain the 1/2-plateau phase [24] that we concentrate on. When $B_z = 0$, the system has the rotational symmetry in the spin space and the time-reversal symmetry, but those symmetries are broken for finite B_z . However, even with finite B_z , the system retains the spatial inversion symmetry, which is essential for protecting the topological phase in the 1/2-plateau phase.

In order to elucidate the topological properties of the model, we calculate the magnetization, the Berry phase, and the entanglement entropy. The magnetization is calculated to show the existence of the plateau phase. The Berry phase defined below works as a symmetry-protected topological order parameter to identify two topologically distinct states having the same symmetry [3]. The entanglement entropy for the spatial bipartition is evaluated to check whether or not the two states can be smoothly connected. Also the entanglement entropy gives a picture of the bulk-edge correspondence because the topological character of the system is encoded

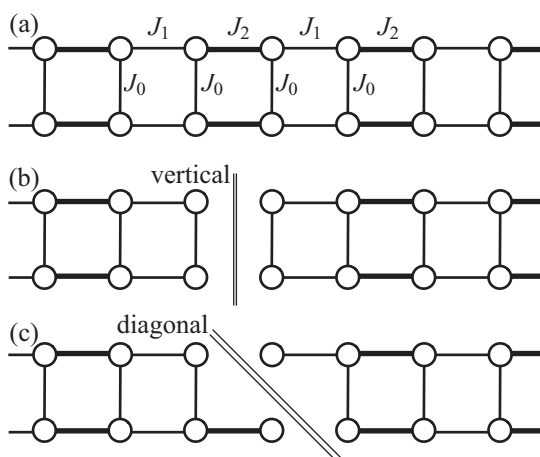


FIG. 1. (a) The dimerized spin-1/2 Heisenberg ladder. Definitions of parameters are shown. (b) The vertical edge. (c) The diagonal edge.

in the entanglement spectrum [25,26], and the entanglement entropy contains a contribution from the edge states [11,27]. Analysis based on the transformation law of the matrices in the matrix product state (MPS) representation is also performed to complement the Berry-phase-based arguments, i.e., we extract a topological order parameter other than the quantized Berry phase from the MPS representation. In addition, by making use of the translationally invariant MPS representation that enables us to access the thermodynamic limit, we can discuss the collapse of the SPT phase with spontaneous symmetry breaking.

Numerical methods

The calculations of the Berry phase and the investigation of the edge states are performed by the exact diagonalization of the finite-size system. The ground-state energy and the wave function are numerically evaluated by the Lanczos algorithm combined with the inverse iteration method. In order to define the Berry phase, we apply a local gauge twist on the bonds (possibly on the multiple bonds) at the given boundary as

$$S_L^+ S_R^- + \text{H.c.} \longrightarrow e^{i\phi} S_L^+ S_R^- + \text{H.c.}, \quad (2)$$

where L and R denote the sites on the left and right sides, respectively, of the given boundary. Using the ground-state wave function $|G_\phi\rangle$ at each ϕ , the Berry phase γ is obtained as

$$i\gamma = \int_0^{2\pi} d\phi \langle G_\phi | \partial_\phi | G_\phi \rangle. \quad (3)$$

In practice, by discretizing the range $[0, 2\pi]$ as $\phi_i = 2\pi i/N$ ($i = 1, \dots, N-1$), it is evaluated as [3,28,29]

$$\gamma = \arg \left(\langle G_{\phi_{N-1}} | G_{\phi_0} \rangle \prod_{i=0}^{N-1} \langle G_{\phi_i} | G_{\phi_{i+1}} \rangle \right). \quad (4)$$

Because the gauge twist is applied on the bonds crossing the boundary, the Berry phase depends on the boundary shape, which is essential for establishing the bulk-edge correspondence [11,30]. With the exact-diagonalization scheme, finite-size effects are unavoidable. However, as long as the Berry phase is quantized due to some symmetry, as we will see below, there is practically no size effect on the numerically obtained Berry phases.

In order to obtain the entanglement entropy and the MPS, the iTEBD method is employed [23]. In the iTEBD, a translationally invariant MPS representation of the ground state is iteratively obtained. It becomes exact in the large- χ limit, where χ is the truncation dimension corresponding to the dimension of the matrix in the MPS representation. For gapped phases, small χ is sufficient to obtain results in practical precision. An advantage of the iTEBD is accessibility to the thermodynamic limit, i.e., it is free from the finite-size effect, because it provides a translationally invariant MPS representation by construction. The finite-size-effect-free nature is essential for discussing spontaneous symmetry breaking. To perform the iTEBD, translation symmetry is essential and the target system is assumed to be composed of the repetition of unit objects. Then, the iTEBD naturally gives entanglement entropy for the bipartition such that the system is divided

into two parts in between the two neighboring unit objects. In the following, unit objects are appropriately chosen so as to make a given boundary in between two of them. In this way, the entanglement entropy depends on the shapes of the given boundary, as it should do.

With the iTEBD, it is possible to obtain the translationally invariant canonical MPS representation [31] of the state such that

$$|\Psi\rangle = \sum_{\{s_i\}} \cdots \Gamma_{s_i} \Lambda \Gamma_{s_{i+1}} \Lambda \cdots |\cdots, s_i, s_{i+1}, \cdots\rangle, \quad (5)$$

where s_i denotes the labels of local states, and Γ_s and Λ are $\chi \times \chi$ matrices. Λ is a diagonal matrix whose entries are non-negative and related to the entanglement entropy S as

$$S = - \sum_i \lambda_i^2 \ln \lambda_i^2, \quad (6)$$

where λ_i is the diagonal elements of Λ . When $|\Psi\rangle$ respects some symmetry, Γ_s must react against the symmetry operation appropriately. Then, physical states with the same symmetry can be classified by this transformation law of Γ_s . When the symmetry operation is written by a product of local operators $O^{(a)}$, $\Gamma_{s'}$ transforms as [32]

$$\sum_{s'} O_{ss'}^{(a)} \Gamma_{s'} = e^{i\theta_a} U_a^\dagger \Gamma_s U_a, \quad (7)$$

where U_a is an unitary matrix that satisfies $[\Lambda, U_a] = 0$. Mathematically, U_a gives a projective representation of the symmetry operation and the states are distinguished by its factor set [25,33,34]. If the operation involves the spatial inversion symmetry, which plays a central role in this paper, then $\Gamma_{s'}$ at the left-hand side of Eq. (7) is replaced by ${}^t\Gamma_{s'}$, which is the transpose of $\Gamma_{s'}$ [25], since the inversion operation reverses the order of s_i . In general, a cyclic group generated by a single element, such as the case that there is only inversion symmetry, leads to no interesting factor set. However, this transposition makes the inversion symmetry useful in the classification of the states. Namely, there is a restriction on U_a for the spatial inversion symmetry (denoted as U_I hereafter) such that ${}^tU_I = \pm U_I$, which means that U_I should be symmetric or antisymmetric [25]. For antisymmetric U_I , the relation $[\Lambda, U_I] = 0$ gives degeneracy of the entanglement spectrum, in which the topological properties of the system are encoded [25]. Particularly, if the entanglement spectrum is at least doubly degenerate, the entanglement entropy has a lower bound, $\ln 2$. As we will focus on the phase with the finite magnetic field, in which the time-reversal symmetry and the symmetries in the spin space are not effective, ζ , which is defined according to

$${}^tU_I = \zeta U_I, \quad (8)$$

and takes values of $+1$ and -1 , is employed as a topological order parameter to classify the phases.

In practice, U_I is obtained as an ‘‘eigenmatrix’’ of a linear matrix map [32],

$$\mathcal{E}_I(U) = \sum_{ss'} \hat{O}_{ss'}^{(I)} ({}^t\Gamma_s \Lambda) U (\Gamma_{s'} \Lambda)^\dagger, \quad (9)$$

whose eigenvalue ϵ satisfies $|\epsilon| = 1$. Specifically, U_I satisfies

$$\mathcal{E}_I(U_I) = e^{i\theta} U_I. \quad (10)$$

Numerically, $e^{i\theta}$ and U_I are obtained as an eigenvalue and an eigenvector of the matrix representation of the map \mathcal{E}_I , whose matrix elements are defined as

$$T_{ij:i'j'} = \sum_{ss'} \hat{O}_{ss'}^{(I)} ({}^t\Gamma_s)_{ii'} \lambda_i ({}^t\Gamma_{s'})_{jj'}^* \lambda_{j'}. \quad (11)$$

The matrix T works as a transfer matrix when we calculate the overlap between the wave functions before and after the symmetry operation is applied [33]. It means that, as far as the state respects the symmetry, the largest norm of the eigenvalues of T becomes unity. Then, U_I is obtained from an eigenvector associated with the eigenvalue with unit norm, and ζ is reduced from it. On the other hand, if the largest norm of the eigenvalues of T is less than unity, it implies that the state under consideration does not respect the symmetry. In other words, T has an ability to detect whether a given state is invariant against a symmetry operation. For convenience, we set ζ to zero when T detects a symmetry breaking and U_I is unavailable.

III. RESULTS AND DISCUSSIONS

The magnetization curve obtained with the iTEBD for $J_0 = 1.0$, $J_1 = 1.0 - \Delta$, and $J_2 = 1.0 + \Delta$ with several values of Δ is shown in Fig. 2. The essential features of the curves are consistent with those in Ref. [15]. Namely, there are two plateau phases, for $\langle S_z \rangle = 0$ (0 plateau) and $\langle S_z \rangle = 1/4$ (1/2 plateau). The width of the 1/2 plateau depends on the strength of the dimerization Δ . If there is no dimerization, the unit cell contains only two sublattices, and the plateau at $\langle S_z \rangle = 1/4$, which is a half of the saturation magnetization, is not allowed. On the other hand, the 0-plateau phase does not vanish in the zero dimerization limit. This is natural because the 0-plateau phase without dimerization is actually in the rung singlet phase [35,36], and the rung singlet is expected to be stable for small dimerization.

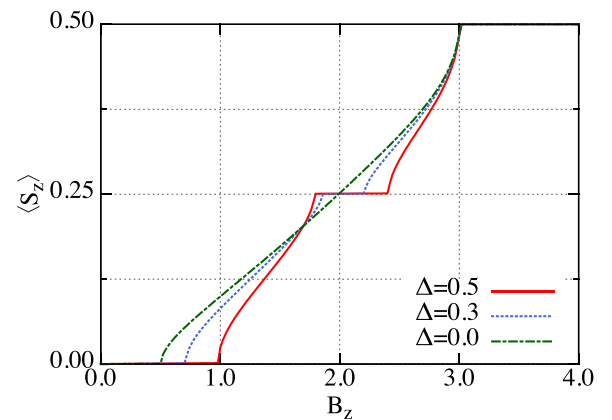


FIG. 2. (Color online) The magnetization curve for $\Delta = 0.0, 0.3$, and 0.5 obtained with $\chi = 24$. Magnetization is already converged with $\chi = 24$ or smaller.

A. Topological order parameter in the 1/2-plateau phase

Let us move on to the topological properties of the 1/2-plateau phase. Figures 3(a) and 3(b) show the numerically obtained Berry phase and entanglement entropy for the 1/2-plateau phase. These quantities depend on the boundary shape, and the vertical edge in Fig. 1(b) is employed here. (Later we will discuss the edge states and then the diagonal edge is also used.) What is important is that the vertical edge does not break the inversion symmetry whose inversion center is at the boundary. Then, the Berry phase is quantized into 0 or π , as in Fig. 3(b). This quantization is caused by the spatial inversion symmetry [30]. Here, the inversion symmetry means that the Hamiltonian with the gauge twist ϕ satisfies

$$\hat{H}_{-\phi} = \hat{P}^{-1} \hat{H}_{\phi} \hat{P}, \quad (12)$$

where \hat{P} is an appropriate unitary matrix. This relation combined with the assumption that the ground state is unique implies $\gamma = -\gamma \pmod{2\pi}$, which immediately leads to the quantization of γ into 0 or π . As this quantization is robust provided that the spatial inversion symmetry is kept intact, γ can be regarded as a symmetry-protected topological order parameter. The Berry phase γ shows a jump at $\Delta = 0$, which suggests a phase transition. This phase transition is also detected by the entanglement entropy as its divergent behavior.

Analysis of the transformation law of Γ_s also supports this conclusion. In fact, as is shown in Fig. 3(c), ζ is 1 for $\Delta < 0$ and -1 for $\Delta > 0$, which confirms that both states

respect the spatial inversion symmetry, but are topologically distinct from each other. For $\Delta > 0$, the entanglement entropy is always larger than $\ln 2$, due to the double degeneracy of the entanglement spectrum that is associated with $\zeta = -1$. Importantly, $\zeta = -1$ is found in the phase with $\gamma = \pi$, which implies consistency between γ and ζ as a topological order parameter. Since we are considering the finite B_z case, the time-reversal symmetry and the rotational symmetry in spin space cannot be used here.

For this classification of the phases, the choice of the position of the boundary is essential because the states with $\Delta > 0$ and those with $\Delta < 0$ are equivalent by a single-site translation of the whole system. This means that the observed transition is similar to that of the Su-Schrieffer-Heeger model [37] or the dimerized spin-1/2 Heisenberg chain [38–41]. A relation to the dimerized chain is understood by considering the strong rung coupling limit, though our calculation so far assumes the comparable rung and leg couplings. The spin-1/2 ladder in the strong rung coupling limit at $\langle S_z \rangle = 1/4$ is effectively described by a XXZ chain model at zero magnetization with easy-plane anisotropy [14,42,43]. Then, the present phase under consideration is expected to be connected to the phase of the dimerized XXZ chain. On the other hand, the dimerized XXZ chain with easy-plane anisotropy is smoothly connected to the anisotropic chain. (This is not the case with the easy axis, or Ising, anisotropy since the system will be in an antiferromagnetic phase at least for the weak dimerization limit.) Now, we confirm that the transition in Fig. 3 is the same type as the transition in the dimerized spin-1/2 chain with no external magnetic field [40,41], where two distinct phases are distinguished by the positions of spin singlets.

B. Role of the symmetry in protecting the topological phases

In the previous section, the states are characterized by the Z_2 Berry phase (and the transformation law of Γ_s). In order to demonstrate the role of the symmetry, we introduce a symmetry-breaking term and show that the two phases are continuously connected if the symmetry is broken. Here, we add a term

$$\hat{H}_{\text{artificial}} = \delta J_0 \sum_{i=1}^{2L} (-1)^i \mathbf{S}_{i,1} \cdot \mathbf{S}_{i,2}, \quad (13)$$

which makes staggered modulation of the rung coupling [44–46] and breaks the spatial inversion symmetry whose inversion center is in between the two rungs. Parameters η and α are introduced as

$$\Delta = \eta - 0.5, \quad (14)$$

$$\delta J_0 = \alpha \eta (1 - \eta). \quad (15)$$

With this definition, the states with $\eta = 0$ ($\Delta = -0.5$, $\delta J_0 = 0$) and $\eta = 1$ ($\Delta = 0.5$, $\delta J_0 = 0$) retain the spatial inversion symmetry. The Berry phase and the entanglement entropy for several α in the 1/2-plateau phase are shown in Fig. 4. The Berry phase is no longer quantized and the jump observed in Fig. 3 is removed. (In principle, the finite-size effects come into play in this case without quantization, but in the present case, the results obtained with the 20 spin system and the 24 spin

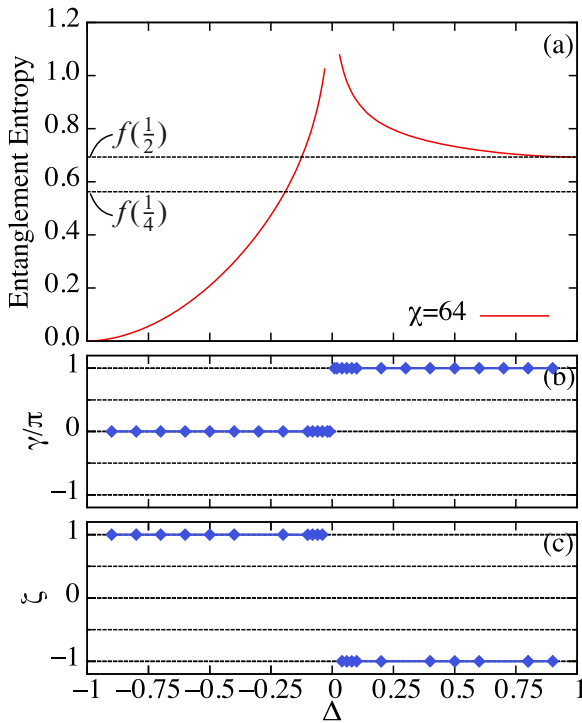


FIG. 3. (Color online) (a) The entanglement entropy, (b) the Berry phase, and (c) the other topological order parameter ζ as a function of Δ for the vertical edge. The entanglement entropy is calculated with $B_z = 2.0$ and $\chi = 64$. The Berry phase is obtained with the $\langle S_z \rangle = 1/4$ sector in the six unit cell (24 spins) system. ζ is calculated with $\chi = 32$.

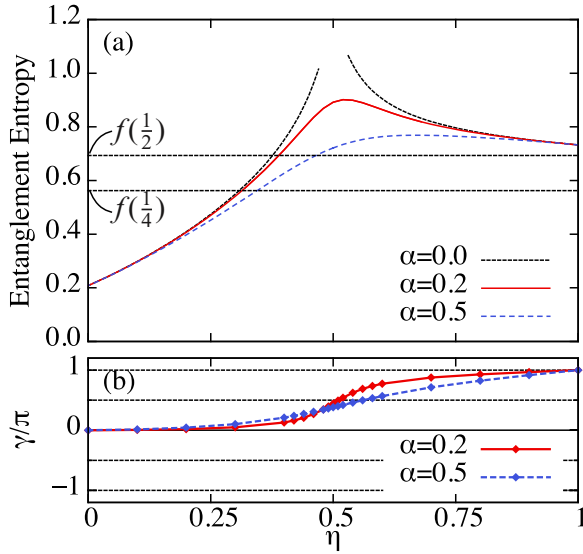


FIG. 4. (Color online) (a) The entanglement entropy and (b) the Berry phase with artificial symmetry breaking. The entanglement entropy for $\alpha = 0.2$ and 0.5 is obtained with $B_z = 2.0$ and $\chi = 24$. The Berry phase is calculated with the $\langle S_z \rangle = 1/4$ sector of six unit cell (24 spins) system.

system are nearly identical.) At the same time, divergence in the entanglement entropy is also removed, similar to the case of the symmetry-broken dimerized chain [41]. Furthermore, $\zeta = 0$ since the maximum norm of the eigenvalues of T is less than unity, as it should be with the broken spatial inversion symmetry. All of these results are consistent with the crucial role of the symmetry. Two kinds of symmetry-protected topological order parameters, γ and ζ , which pick up the same information when the inversion symmetry exists, give quite different information when the inversion symmetry is broken. By definition, ζ is set to zero in such a case. On the other hand, γ takes some value and works as a measure of the “distance” to the topological phase or the trivial phase.

C. Bulk-edge correspondence for a symmetry-preserving boundary

Next, we move on to the analysis of the edge states to see the bulk-edge correspondence. In the following, we see that the $\gamma = \pi$ ($\zeta = -1$) state shows a clear sign of an edge state, while the $\gamma = 0$ ($\zeta = 1$) state does not. Figure 5 shows the site-resolved magnetization of the ground state obtained with

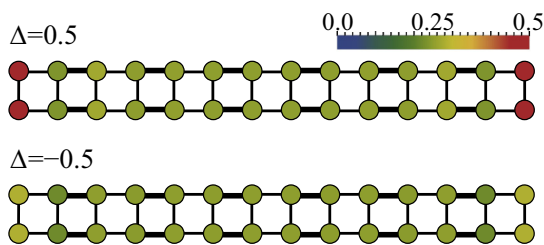


FIG. 5. (Color online) Site-resolved magnetization with the vertical open boundary for $\Delta = 0.5$ (upper panel) and $\Delta = -0.5$ (lower panel).

the open boundary. For this calculation, we used $\Delta = \pm 0.5$ and $B_z = 2.0$. For $\Delta = 0.5$, the total magnetization of the ground state deviates from exactly being $\langle S_z \rangle = 1/4$, but the ground state has one more extra up spin. This extra up spin is localized at the boundary, as we can see from Fig. 5, which makes the edge distinct from the bulk. No significant change of the local magnetization is found in the bulk part. On the other hand, for $\Delta = -0.5$, the ground-state magnetization exactly satisfies $\langle S_z \rangle = 1/4$ and the local magnetization is only weakly affected at the boundary. These behaviors are clearly explained in the $\Delta = \pm 1$ limit, i.e., the decoupled limit. In this limit, we only have to consider the four-site clusters. For $\Delta = -1$, the boundary does not break a cluster, and we expect no edge states. On the other hand, for $\Delta = 1$, a cluster at the boundary is broken and the lowest energies of the broken cluster at each magnetization are obtained as $-2B_z + J_0/2$ ($\langle S_z \rangle = 1/2$), $-B_z - J_0/2$ ($\langle S_z \rangle = 1/4$), and $-3J_0/2$ ($\langle S_z \rangle = 0$). In the present case, $J_0 = 1.0$ and $B_z = 2$, the fully polarized state ($\langle S_z \rangle = 1/2$) is chosen at the boundary, which indicates that the extra up spin is localized at the boundary. The $\Delta = \pm 0.5$ cases are adiabatically connected to the case with $\Delta = \pm 1$.

The existence of the edge states is also reflected in the entanglement entropy. This point is clarified by considering $\Delta = \pm 1$. In this case, it is easy to evaluate the entanglement entropy because we only have to take account of the entanglement within a single four-site cluster. For $\langle S_z \rangle = 1/4$ and $\Delta = 1$, the resultant entanglement entropy is $f(1/2)$, where $f(x) = -x \ln x - (1-x) \ln(1-x)$ (see the Appendix). For $\Delta = 1$, because of $\zeta = -1$, the degeneracy of the entanglement spectrum is expected, and $f(1/2) = \ln 2$ is consistent with the lower bound set by the degeneracy. On the other hand, for $\Delta = -1$, where no edge state is expected, the entanglement entropy is zero, since the cluster is not broken. In fact, the numerical result in Fig. 3(a) shows that the entanglement entropy approaches these values in the $\Delta = \pm 1$ limit. In short, the entanglement entropy in the positive Δ side is largely contributed from the edge state.

D. Symmetry-breaking boundary and fractional quantization of the Berry phase

So far, we have only considered the vertical edge. Now, let us move on to the diagonal edge [see Fig. 1(c)]. An important feature of the diagonal edge is that it breaks the inversion symmetry no matter where we choose as the inversion center, even if the bulk symmetry is kept intact. (Recall that the vertical edge keeps the inversion symmetry if we set the inversion center at the boundary.) Even in this case, since the bulk symmetry is preserved and the Berry phase and the entanglement entropy are bulk quantities, i.e., both quantities are obtained by bulk ground-state wave functions, these quantities still have an ability to sense a topological phase transition. But, of course, they should behave differently from the case of the symmetry-preserving boundary. For instance, the Berry phase need not be quantized into 0 or π , and is not necessarily useful in a naive thought. However, in the present model, the diagonal edge also exhibits interesting phenomena, as shown below. First, the Berry phase for the diagonal edge in the $1/2$ -plateau phase is shown in Fig. 6. There, we can see that

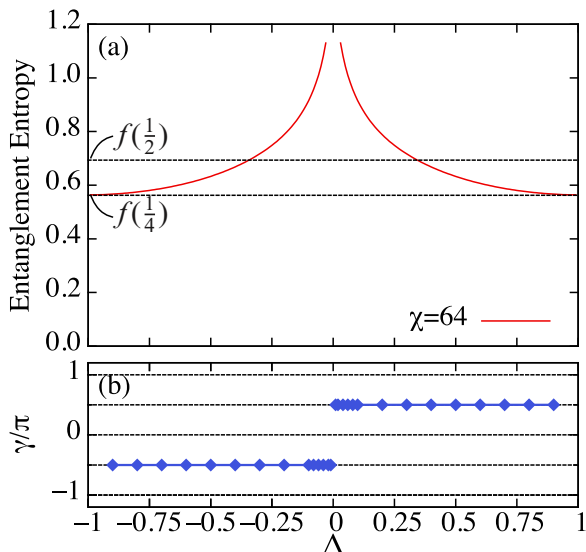


FIG. 6. (Color online) (a) The entanglement entropy and (b) the Berry phase for the diagonal edge. The entanglement entropy is calculated with $B_z = 2.0$ and $\chi = 64$. The Berry phase is obtained using the system with six unit cells (24 spins) with $\langle S_z \rangle = 1/4$.

the Berry phase is quantized into $\pm\pi/2$, that is, the Berry phase shows the unique fractional quantization [11]. This fractional quantization comes from the formula

$$\gamma_{\text{diagonal}} = \gamma_{\text{vertical}} - 2\pi(S - \langle S_z \rangle), \quad (16)$$

derived in a similar way as in Refs. [11] or [29]. Since γ_{vertical} is quantized into 0 or π by the spatial inversion symmetry, and $\langle S_z \rangle$ is fixed to $1/4$ owing to the symmetry of the model, γ_{diagonal} is quantized into $\pm\pi/2$. Figure 6(b) indicates that the topological phase transition is captured as a jump in γ since the bulk symmetry is kept, but $0/\pi$ quantization is broken because of the symmetry-breaking boundary.

The entanglement entropy is also plotted in Fig. 6. Different from the case of $0/\pi$ quantization, the entanglement entropy is finite in both of the positive and negative sides of the $\Delta = \pm 1$ limit. As in the case of the vertical edge, the entanglement entropy is obtained for $\Delta = \pm 1$ as $f(1/4)$ (see the Appendix). Although the topological phase transition is detected as a diverging behavior due to the bulk nature of the entanglement entropy, degeneracy of the entanglement entropy originating from the inversion symmetry does not take place for the symmetry-breaking boundary and we have a situation in which the entanglement entropy becomes smaller than $\ln 2$, for instance, $f(1/4) < f(1/2) = \ln 2$. This behavior is confirmed in Fig. 6.

Now we investigate the open ladder with the diagonal edge to see the bulk-edge correspondence for the $\pm\pi/2$ quantization case. In Fig. 7, the site-resolved $\langle S_z \rangle$ for the ground state of $\langle S_z \rangle = 1/4$ sector with $\Delta = 0.5$ is plotted. There, the extra up spins are accumulated at the left edge, while the extra down spins are accumulated at the right edge. For negative Δ , where the edge states are not observed for the case with $0/\pi$ quantization, there are still edge states, but the roles of the right and the left edges are reversed. This is consistent with the fact that the entanglement entropy goes to finite values for

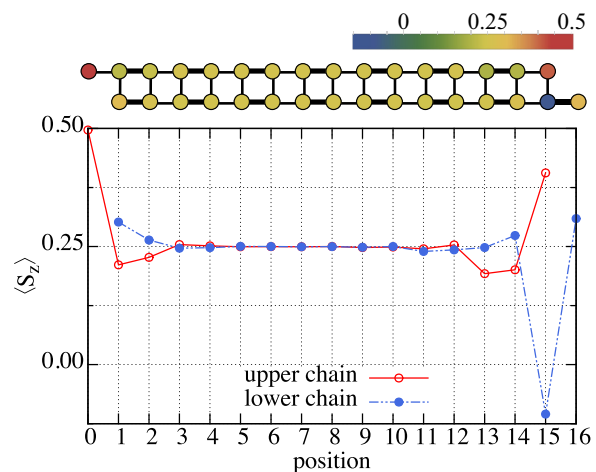


FIG. 7. (Color online) The site-resolved spin density in the $1/2$ -plateau phase with the diagonal edge. The color map of the spin density is also shown. Calculation is performed on the system with 32 spins.

both $\Delta = \pm 1$. To summarize, the edge states for the $\pm\pi/2$ quantization have features such that (i) the up and down spins are accumulated at the opposite ends, and (ii) the edge states appear both for positive and negative Δ . These features give a physical picture of the $\pm\pi/2$ quantization. First, since $+\pi/2$ and $-\pi/2$ differ only in sign and have the same magnitudes, we expect the similar behavior of the edge states for positive and negative Δ , which explains feature (ii). This makes a clear contrast to the case of $0/\pi$ quantization, where 0 and π are essentially different, and leads to the absence and existence of the edge states. To understand feature (i), analogy to the electron system is helpful. In free-electron systems, there is a direct relation between the electronic polarization and the Berry phase [47]. By regarding up spins as electrons and down spins as holes, the state in Fig. 7 corresponds to the electronically polarized state associated with the finite Berry phase. Note that $\gamma = \pi$ represents the situation where the mean position of the electrons is at the middle point between two lattice points, which means that there is no electronic polarization even though the Berry phase is finite. Thus, the quantization into $\pm\pi/2$ instead of $0/\pi$ is essential to observe feature (i).

In order to observe a unique quantization of the Berry phase described above, the ladder structure and the applied magnetic field are essential. First of all, the ladder structure allows us to consider the diagonal edge for which the fractional quantization is achieved. Further, Eq. (16) implies that we need to look at the plateau phase with $\langle S_z \rangle = 1/4$ to have the fractional quantization. Although the plateau phase under consideration can be mapped to the zero magnetization phase in the XXZ chain in the strong rung coupling limit, the fractional quantization is not expected in the XXZ chain since it does not admit the diagonal edge.

E. Ring exchange

So far, we have considered the $1/2$ -plateau phase induced by the dimerization. For the uniform case without dimerization, a plateau phase at the same magnetization $\langle S_z \rangle = 1/4$

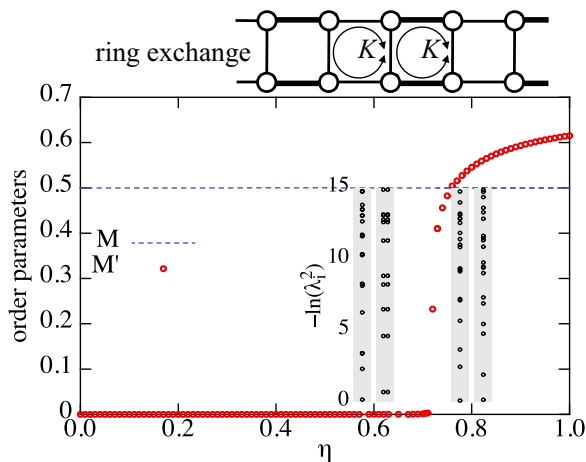


FIG. 8. (Color online) Order parameters M and M' obtained with $B_z = 2.0$ and $\chi = 48$. Insets: The entanglement spectra for $\eta = 0.6$ and 0.8 . For each value of η , the left column is for the edge on the J_1 bond and the right column is for the edge on the J_2 bond.

is induced by a ring exchange [43,48], which is written as [19,20,35,43,49]

$$\hat{H}_{\text{ring}} = K \sum_i (P_i + P_i^{-1}), \quad (17)$$

where P_i (P_i^{-1}) is an operator acting on the minimal four-site plaquette that causes a clockwise (anticlockwise) shift of the spins on that plaquette. That is, if we denote the states of four spins on a plaquette as $\begin{pmatrix} s_1 & s_2 \\ s_3 & s_4 \end{pmatrix}$, then P_i operates as

$$P_i \begin{pmatrix} s_1 & s_2 \\ s_3 & s_4 \end{pmatrix} = \begin{pmatrix} s_2 & s_4 \\ s_1 & s_3 \end{pmatrix}, \quad P_i^{-1} \begin{pmatrix} s_1 & s_2 \\ s_3 & s_4 \end{pmatrix} = \begin{pmatrix} s_3 & s_1 \\ s_4 & s_2 \end{pmatrix}. \quad (18)$$

Intuitive understanding of the ring exchange is possible for the strong rung coupling limit. There, we have noted that the model is effectively described by a XXZ chain model. The ring exchange term modifies the anisotropy of the effective XXZ model, i.e., the anisotropy is modified from the easy-plane type to the easy-axis type (Ising type) for sufficiently large positive K . Then, the antiferromagnetic order is developed in the effective model, and this ordered phase corresponds to the $1/2$ -plateau phase in the original model [43]. Due to the antiferromagnetic nature of the state, the spatial inversion symmetry that is essential for the SPT phase is broken. Then, a transition between the SPT phase and the symmetry-broken phase *within the $1/2$ -plateau phase* is expected when the strength of the ring exchange is suitably tuned. In fact, such a transition is observed in the present model. In Fig. 8, $M = \frac{1}{2L} \sum_i^{2L} \sum_{j=1,2} \langle S_{i,j}^z \rangle$, and $M' = \frac{1}{2L} \sum_i^{2L} \sum_{j=1,2} (-1)^i \langle S_{i,j}^z \rangle$, which captures the symmetry breaking, are plotted as a function of η introduced as $\Delta = 0.2(1 - \eta)$ and $K = 0.8\eta$. Note that the dimerization-dominated plateau phase is expected for $\eta = 0$, while the ring-exchange-dominated plateau phase is expected for $\eta = 1$. The numerical result in Fig. 8 confirms this idea. Namely, M' gets finite at a certain value of η as η increases, while M is always 0.5.

In order to clarify the difference between zero M' phase and finite M' phase in terms of SPT, the entanglement spectra for $\eta = 0.6$ and 0.8 are also shown in Fig. 8. We did not

use the Berry phase since it requires a finite-size system for calculation, which means that it is difficult to treat the phase with spontaneous symmetry breaking. Here, we only use the vertical edges. Still, there are two choices of the vertical edges, i.e., one breaks J_1 bonds and the other breaks J_2 bonds. Therefore, for each value of η , two spectra are plotted. At $\eta = 0.6$, we observe double degeneracy of the spectrum for the edge on J_2 bonds. This degeneracy stems from the nontrivial projective representation, $\zeta = -1$, and signals a SPT phase. On the other hand, for $\eta = 0.8$, neither of the edges on J_1 and J_2 bonds leads to the degeneracy of the spectra. This observation implies that the transition in Fig. 8 is a typical and concrete example for the collapse of the SPT phase by a spontaneous symmetry breaking.

E. Comparison with the 0-plateau phase

Finally, we briefly discuss the 0-plateau phase near zero magnetic field. In this case, there is no sign of the phase transition in both of the Berry phases and the entanglement entropy plotted as a function of Δ (not shown). This is natural because the $\Delta = 0$ state is not critical, but is described as a rung singlet state [35,36] without the Zeeman field. In contrast, the dimerized *chain* is critical when $\Delta = 0$ and $B_z = 0$. However, actually, there is no jump at $\Delta = 0$ in the Berry phase as a function of Δ , even in the small rung coupling limit. This is because we apply gauge twists on *all* bonds across the boundary. Then, even for Δ for which a topologically nontrivial phase is expected in the dimerized *chain*, the Berry phase is 0 for the dimerized ladder because each chain contributes π to γ , which results in $\gamma = 2\pi \equiv 0 \pmod{2\pi}$. If we apply different kinds of gauge twist, not limited to the one that is possible to be reduced to a twisted boundary condition, it is possible to detect dimer structures [19,20,50]. We have also confirmed the absence of the topological phase protected by the spatial inversion symmetry in the 0-plateau phase by the MPS representation. That is, in the 0-plateau phase, ζ is always 1, irrespective of the sign of Δ .

IV. SUMMARY

To summarize, it is established that there is a symmetry-protected topological phase in the $1/2$ -plateau phase in the dimerized spin- $1/2$ Heisenberg ladder. Even with the magnetic field, which is necessary to access the $1/2$ -plateau phase and reduces the symmetry of the system, the spatial inversion symmetry remains and protects the topological phase. Namely, the inversion symmetry makes the Berry phase quantized into 0 or π , and allows us to regard the Berry phase as a topological order parameter. The entanglement entropy is also used to characterize the topological phase. In order to complement the Berry-phase-based arguments, the topological order parameter other than the Berry phase is extracted from the MPS representation of the state. That topological order parameter determines the degeneracy of the entanglement spectrum and gives lower bound of the entanglement entropy. The importance of the symmetry is demonstrated by introducing a symmetry-breaking term and by spontaneous symmetry breaking caused by the ring exchange. Because of the importance of the inversion symmetry, the boundary

that respects the inversion symmetry is mainly used to define the Berry phase and the entanglement entropy. However, our analysis on a specific shape of boundary reveals that the symmetry-breaking boundary can lead to a different type of bulk-edge correspondence. Specifically, we find a fractional quantization of the Berry phase into $\pm\pi/2$ for such a symmetry-breaking boundary. Further it is shown that there are unique edge states, which show polarization, i.e., up and down spins are accumulated at the opposite ends of the finite system, for the case with $\pm\pi/2$ quantization. This finding implies new possible applications of the Berry phase for exploring the topological properties of given systems. For instance, the idea of the fractional quantization of the Berry phase will have some applications also in two- or three-dimensional systems in the magnetic fields. Other types of the fractional quantization can be possible for the different plateau phases.

ACKNOWLEDGMENTS

This work is partly supported by Grants-in-Aid for Scientific Research, No. 26247064 and No. 25610101 from JSPS, and Grant No. 25107005 from MEXT. The authors thank the Supercomputer Center, the Institute for Solid State Physics, the University of Tokyo for the use of the facilities.

APPENDIX: ANALYTICAL CALCULATION OF THE ENTANGLEMENT ENTROPY FOR A DECOUPLED FOUR-SITE CLUSTER

1. Hamiltonian and ground state

For a four-site plaquette with $\langle S_z \rangle = 1/4$, there are four basis states written as

$$\begin{aligned} |\text{I}\rangle &= \begin{vmatrix} \uparrow & \uparrow \\ \uparrow & \downarrow \end{vmatrix}, & |\text{II}\rangle &= \begin{vmatrix} \uparrow & \uparrow \\ \downarrow & \uparrow \end{vmatrix}, \\ |\text{III}\rangle &= \begin{vmatrix} \uparrow & \downarrow \\ \uparrow & \uparrow \end{vmatrix}, & |\text{IV}\rangle &= \begin{vmatrix} \downarrow & \uparrow \\ \uparrow & \uparrow \end{vmatrix}. \end{aligned} \quad (\text{A1})$$

The Hamiltonian of the plaquette acts on these basis states as

$$\hat{H}_p |\text{I}\rangle = \frac{J_1}{2} |\text{II}\rangle + \frac{J_0}{2} |\text{III}\rangle, \quad (\text{A2})$$

$$\hat{H}_p |\text{II}\rangle = \frac{J_1}{2} |\text{I}\rangle + \frac{J_0}{2} |\text{IV}\rangle, \quad (\text{A3})$$

$$\hat{H}_p |\text{III}\rangle = \frac{J_1}{2} |\text{IV}\rangle + \frac{J_0}{2} |\text{I}\rangle, \quad (\text{A4})$$

$$\hat{H}_p |\text{IV}\rangle = \frac{J_1}{2} |\text{III}\rangle + \frac{J_0}{2} |\text{II}\rangle. \quad (\text{A5})$$

If $J_1 > 0$ and $J_0 > 0$, the ground state is obtained as

$$|G\rangle = \frac{1}{2} (|\text{I}\rangle - |\text{II}\rangle - |\text{III}\rangle + |\text{IV}\rangle). \quad (\text{A6})$$

2. Entanglement entropy

For a given bipartition, a state is expressed as

$$|\psi\rangle = \sum_{ij} M_{ij} |\psi_i^{\leftarrow}\rangle \otimes |\psi_j^{\rightarrow}\rangle, \quad (\text{A7})$$

where each of $|\psi_i^{\leftarrow}\rangle$ and $|\psi_j^{\rightarrow}\rangle$ is a state in either part of the bipartitioned system. Using the singular value decomposition, a matrix \hat{M} can always be written as

$$\hat{M} = \hat{U} \hat{\Lambda} \hat{V}^\dagger, \quad (\text{A8})$$

where $\hat{\Lambda}$ is a diagonal matrix whose elements are non-negative, and \hat{U} and \hat{V} are unitary matrices. Then, $|\psi\rangle$ is rewritten as

$$|\psi\rangle = \sum_{\alpha} \lambda_{\alpha} |\tilde{\psi}_{\alpha}^{\leftarrow}\rangle \otimes |\tilde{\psi}_{\alpha}^{\rightarrow}\rangle, \quad (\text{A9})$$

with

$$|\tilde{\psi}_{\alpha}^{\leftarrow}\rangle = \sum_i U_{i\alpha} |\psi_i^{\leftarrow}\rangle, \quad |\tilde{\psi}_{\alpha}^{\rightarrow}\rangle = \sum_j (V^\dagger)_{\alpha j} |\psi_j^{\rightarrow}\rangle, \quad (\text{A10})$$

where λ_{α} denotes the diagonal elements of $\hat{\Lambda}$.

The entanglement entropy for this bipartition is evaluated as

$$S = - \sum_{\alpha} \lambda_{\alpha}^2 \ln \lambda_{\alpha}^2. \quad (\text{A11})$$

3. Entanglement entropy for a plaquette

First, we consider the vertical edge that breaks a four-site plaquette into two parts with two spins. Taking a set

$$\begin{vmatrix} \uparrow \\ \uparrow \end{vmatrix}, \quad \begin{vmatrix} \uparrow \\ \downarrow \end{vmatrix}, \quad \begin{vmatrix} \downarrow \\ \uparrow \end{vmatrix}, \quad \begin{vmatrix} \downarrow \\ \downarrow \end{vmatrix}, \quad (\text{A12})$$

as $|\psi_i^{\leftarrow}\rangle$ and $|\psi_j^{\rightarrow}\rangle$, $|G\rangle$ can be written in the form of Eq. (A7), with \hat{M} being

$$\hat{M} = \begin{pmatrix} 0 & \frac{1}{2} & -\frac{1}{2} & 0 \\ -\frac{1}{2} & 0 & 0 & 0 \\ \frac{1}{2} & 0 & 0 & 0 \\ 0 & 0 & 0 & 0 \end{pmatrix}. \quad (\text{A13})$$

Then, it is straightforward to confirm that \hat{U} , \hat{V}^\dagger , and $\hat{\Lambda}$ for this case become

$$\hat{U} = \begin{pmatrix} -\frac{1}{\sqrt{2}} & -\frac{1}{2} & \frac{1}{2} & 0 \\ \frac{1}{\sqrt{2}} & -\frac{1}{2} & \frac{1}{2} & 0 \\ 0 & \frac{1}{\sqrt{2}} & \frac{1}{\sqrt{2}} & 0 \\ 0 & 0 & 0 & 1 \end{pmatrix}, \quad \hat{V}^\dagger = \begin{pmatrix} \frac{1}{\sqrt{2}} & \frac{1}{\sqrt{2}} & 0 & 0 \\ -\frac{1}{2} & \frac{1}{2} & \frac{1}{\sqrt{2}} & 0 \\ \frac{1}{2} & -\frac{1}{2} & \frac{1}{\sqrt{2}} & 0 \\ 0 & 0 & 0 & 1 \end{pmatrix}, \quad (\text{A14})$$

and

$$\hat{\Lambda} = \begin{pmatrix} \frac{1}{\sqrt{2}} & 0 & 0 & 0 \\ 0 & \frac{1}{\sqrt{2}} & 0 & 0 \\ 0 & 0 & 0 & 0 \\ 0 & 0 & 0 & 0 \end{pmatrix}. \quad (\text{A15})$$

As a result, we have

$$S = -\frac{1}{2} \ln \frac{1}{2} - \frac{1}{2} \ln \frac{1}{2} = \ln 2. \quad (\text{A16})$$

Next, we consider the diagonal edge that breaks a four-site plaquette into two parts, i.e., one with a spin and another with three spins. Taking a set

$$|\uparrow\rangle, |\downarrow\rangle \quad (\text{A17})$$

as $|\psi_i^{\lessgtr}\rangle$ and a set

$$\left| \begin{array}{c} \uparrow \\ \uparrow \end{array} \right\rangle, \left| \begin{array}{c} \uparrow \\ \downarrow \end{array} \right\rangle, \left| \begin{array}{c} \uparrow \\ \uparrow \\ \downarrow \end{array} \right\rangle, \left| \begin{array}{c} \downarrow \\ \uparrow \end{array} \right\rangle \quad (\text{A18})$$

as $|\psi_i^{\gtrless}\rangle, |G\rangle$ is expressed as in the form of Eq. (A7) with

$$\hat{M} = \begin{pmatrix} 0 & \frac{1}{2} & -\frac{1}{2} & \frac{1}{2} \\ -\frac{1}{2} & 0 & 0 & 0 \end{pmatrix}. \quad (\text{A19})$$

Now, it is easy to see that \hat{U} , \hat{V}^\dagger , and $\hat{\Lambda}$ for this case are

$$\hat{U} = \begin{pmatrix} 1 & -1 \\ 0 & 0 \end{pmatrix}, \quad \hat{V}^\dagger = \begin{pmatrix} 1 & 0 & 0 & 0 \\ 0 & \frac{1}{\sqrt{3}} & 0 & \frac{1}{\sqrt{2}} \\ 0 & -\frac{1}{\sqrt{3}} & \frac{1}{\sqrt{2}} & 0 \\ 0 & \frac{1}{\sqrt{3}} & \frac{1}{\sqrt{2}} & -\frac{1}{\sqrt{2}} \end{pmatrix}, \quad (\text{A20})$$

and

$$\hat{\Lambda} = \begin{pmatrix} \frac{1}{2} & 0 & 0 & 0 \\ 0 & \frac{\sqrt{3}}{2} & 0 & 0 \end{pmatrix}. \quad (\text{A21})$$

Then, the entanglement entropy is obtained as

$$S = -\frac{1}{4} \ln \frac{1}{4} - \frac{3}{4} \ln \frac{3}{4}. \quad (\text{A22})$$

To summarize, we have $f(1/2)$ for the vertical edge and $f(1/4)$ for the diagonal edge with $f(x) = -x \ln x - (1-x) \ln(1-x)$.

-
- [1] X. G. Wen, *Phys. Rev. B* **40**, 7387 (1989).
 [2] Y. Hatsugai, *J. Phys. Soc. Jpn.* **74**, 1374 (2005).
 [3] Y. Hatsugai, *J. Phys. Soc. Jpn.* **75**, 123601 (2006).
 [4] D. J. Thouless, *Topological Quantum Numbers in Nonrelativistic Physics* (World Scientific, Singapore, 1998).
 [5] X. Chen, Z.-C. Gu, and X.-G. Wen, *Phys. Rev. B* **82**, 155138 (2010).
 [6] A. P. Schnyder, S. Ryu, A. Furusaki, and A. W. W. Ludwig, *Phys. Rev. B* **78**, 195125 (2008).
 [7] F. Pollmann, E. Berg, A. M. Turner, and M. Oshikawa, *Phys. Rev. B* **85**, 075125 (2012).
 [8] Y. Hatsugai, *Phys. Rev. Lett.* **71**, 3697 (1993).
 [9] S. Ryu and Y. Hatsugai, *Phys. Rev. Lett.* **89**, 077002 (2002).
 [10] Y. Hatsugai, *Solid State Commun.* **149**, 1061 (2009).
 [11] T. Kariyado and Y. Hatsugai, *Phys. Rev. B* **90**, 085132 (2014).
 [12] T. Barnes, E. Dagotto, J. Riera, and E. S. Swanson, *Phys. Rev. B* **47**, 3196 (1993).
 [13] D. C. Cabra, A. Honecker, and P. Pujol, *Phys. Rev. Lett.* **79**, 5126 (1997).
 [14] F. Mila, *Europhys. J. B* **6**, 201 (1998).
 [15] D. C. Cabra and M. D. Grynberg, *Phys. Rev. Lett.* **82**, 1768 (1999).
 [16] E. H. Kim, G. Fáth, J. Sólyom, and D. J. Scalapino, *Phys. Rev. B* **62**, 14965 (2000).
 [17] G. Y. Chitov, B. W. Ramakko, and M. Azzouz, *Phys. Rev. B* **77**, 224433 (2008).
 [18] S. J. Gibson, R. Meyer, and G. Y. Chitov, *Phys. Rev. B* **83**, 104423 (2011).
 [19] I. Maruyama, T. Hirano, and Y. Hatsugai, *Phys. Rev. B* **79**, 115107 (2009).
 [20] M. Arikawa, S. Tanaya, I. Maruyama, and Y. Hatsugai, *Phys. Rev. B* **79**, 205107 (2009).
 [21] Z.-X. Liu, Z.-B. Yang, Y.-J. Han, W. Yi, and X.-G. Wen, *Phys. Rev. B* **86**, 195122 (2012).
 [22] S. Takayoshi, K. Totsuka, and A. Tanaka, *Phys. Rev. B* **91**, 155136 (2015).
 [23] G. Vidal, *Phys. Rev. Lett.* **98**, 070201 (2007).
 [24] M. Oshikawa, M. Yamanaka, and I. Affleck, *Phys. Rev. Lett.* **78**, 1984 (1997).
 [25] F. Pollmann, A. M. Turner, E. Berg, and M. Oshikawa, *Phys. Rev. B* **81**, 064439 (2010).
 [26] A. Chandran, M. Hermanns, N. Regnault, and B. A. Bernevig, *Phys. Rev. B* **84**, 205136 (2011).
 [27] S. Ryu and Y. Hatsugai, *Phys. Rev. B* **73**, 245115 (2006).
 [28] T. Fukui, Y. Hatsugai, and H. Suzuki, *J. Phys. Soc. Jpn.* **74**, 1674 (2005).
 [29] T. Hirano, H. Katsura, and Y. Hatsugai, *Phys. Rev. B* **78**, 054431 (2008).
 [30] T. Kariyado and Y. Hatsugai, *Phys. Rev. B* **88**, 245126 (2013).
 [31] R. Orús and G. Vidal, *Phys. Rev. B* **78**, 155117 (2008).
 [32] D. Pérez-García, M. M. Wolf, M. Sanz, F. Verstraete, and J. I. Cirac, *Phys. Rev. Lett.* **100**, 167202 (2008).
 [33] F. Pollmann and A. M. Turner, *Phys. Rev. B* **86**, 125441 (2012).
 [34] T. Morimoto, H. Ueda, T. Momoi, and A. Furusaki, *Phys. Rev. B* **90**, 235111 (2014).
 [35] A. Läuchli, G. Schmid, and M. Troyer, *Phys. Rev. B* **67**, 100409 (2003).
 [36] J.-L. Song, S.-J. Gu, and H.-Q. Lin, *Phys. Rev. B* **74**, 155119 (2006).
 [37] W. P. Su, J. R. Schrieffer, and A. J. Heeger, *Phys. Rev. Lett.* **42**, 1698 (1979).
 [38] K. Hida, *Phys. Rev. B* **45**, 2207 (1992).
 [39] H.-H. Hung and C.-D. Gong, *Phys. Rev. B* **71**, 054413 (2005).
 [40] H. T. Wang, B. Li, and S. Y. Cho, *Phys. Rev. B* **87**, 054402 (2013).
 [41] R. Haghshenas, A. Langari, and A. T. Rezakhani, *J. Phys. Condens. Matter* **26**, 456001 (2014).
 [42] K. Totsuka, *Phys. Rev. B* **57**, 3454 (1998).
 [43] A. Nakasu, K. Totsuka, Y. Hasegawa, K. Okamoto, and T. Sakai, *J. Phys. Condens. Matter* **13**, 7421 (2001).
 [44] G. I. Japaridze and E. Pogosyan, *J. Phys. Condens. Matter* **18**, 9297 (2006).

- [45] S. Nemati, S. Batebi, and S. Mahdavi, *Europhys. J. B* **83**, 329 (2011).
- [46] R.-X. Li, S.-L. Wang, K.-L. Yao, and H.-H. Fu, *Phys. Lett. A* **377**, 2422 (2013).
- [47] R. D. King-Smith and D. Vanderbilt, *Phys. Rev. B* **47**, 1651 (1993).
- [48] T. Hikihara and S. Yamamoto, *J. Phys. Soc. Jpn.* **77**, 014709 (2008).
- [49] T. Sakai and Y. Hasegawa, *Phys. Rev. B* **60**, 48 (1999).
- [50] N. Chepiga, F. Michaud, and F. Mila, *Phys. Rev. B* **88**, 184418 (2013).